RSC Advances

PAPER

View Article Online
View Journal | View Issue



Cite this: *RSC Adv.*, 2025, **15**, 49353

# Design, synthesis, and biological evaluation of KA7, a novel quinolone-based sorafenib analogue with potent anticancer and immunomodulatory activities

Duaa abuarqoub, *[a] Ahmed Alshaikh, [a] Marwa Mohammad,[a] Hana'a Khalaf,[a] Nour Albaz[a] and Ali Hmedat[b]

Although multi-kinase inhibitors like **sorafenib** remain an important treatment option for advanced malignancies, their toxicity and resistance to treatment are problems. Enhancing its structure by making changes to the scaffold offers a viable way to boost safety and effectiveness. In this study, 2-(4-chlorobenzylamino)-6-(pyridin-4-yloxy) quinolin-4(1*H*)-one (**KA7**), a novel **sorafenib** analogue, is synthesized and biologically evaluated. **KA7** was synthesized by replacing the urea component of **sorafenib** with a quinolone scaffold. Then, **KA7** was characterized by NMR and HRMS. MTT tests were used to calculate the $IC_{50}$ and assess cytotoxicity against breast (MDA-231, MCF-7), glioblastoma (U87), and lung (A549) cancer cells. Flow cytometry was used to evaluate cell death induction (apoptosis/necrosis), cell cycle analysis, and autophagic activity. The analysis of cytokine release in LPS-stimulated THP-1 macrophages allowed for the determination of **KA7**'s immunomodulatory potential. Our results indicated that **KA7** exhibited $IC_{50}$ values lower than those of **sorafenib** in both U87 and A549 cells, with similar effects observed in MCF-7 cells, demonstrating dose-dependent cytotoxicity. Flow cytometry also revealed a significant increase in apoptosis and G1 phase cell cycle arrest across all cancer cell lines tested. Autophagy induced by **KA7** was confirmed through acridine orange staining. In the macrophage model, **KA7** increased levels of anti-inflammatory cytokines (IL-8 and IL-10) while decreasing pro-inflammatory cytokines (IL-1β, TNF-α, and IL-6), supporting an immunomodulatory profile akin to that of **sorafenib**. In conclusion, **KA7** exhibits strong anticancer properties, inducing apoptosis, arresting the G1 cell cycle, stimulating autophagy, and displaying positive immunomodulatory effects. According to these results, **KA7** is a promising lead chemical for additional preclinical testing as a potent **sorafenib** substitute.

Received 1st October 2025
Accepted 1st December 2025

DOI: 10.1039/d5ra07478a

rsc.li/rsc-advances



## Introduction

Cancer remains one of the leading causes of death worldwide, with lung, stomach, liver, colon, and breast cancers accounting for the majority of cancer-related mortality. This urgent global health challenge underscores the critical need for the discovery and development of novel therapeutic agents with improved efficacy and safety profiles.

**Sorafenib** (Fig. 1) is an FDA-approved oral multikinase inhibitor currently used in the treatment of renal cell carcinoma (RCC), advanced hepatocellular carcinoma (HCC), and thyroid cancer.[1–6] Its therapeutic efficacy arises from its ability to inhibit multiple signaling pathways involved in tumor progression, including vascular endothelial growth factor receptors (VEGFR),[7,8] B-RAF serine/threonine kinase, Ras protein and Ras-mutation[9,10] and mitogen-activated protein kinase (MAPK) pathway.[11]

Despite its clinical success, **sorafenib**'s broad kinase inhibition is also associated with severe adverse effects such as hand–foot skin reaction, diarrhea, hypertension, and fatigue.[12] Thus, there remains a pressing need for safer and more effective targeted therapies. The elucidation of **sorafenib**'s structure and anticancer properties has spurred efforts to optimize its pharmacological profile and to identify analogues with improved

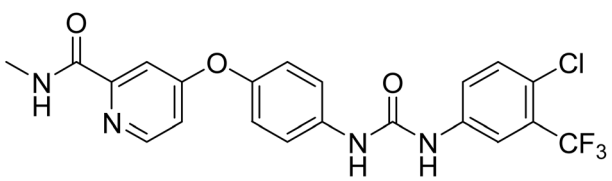


**Sorafenib**

Fig. 1 The chemical structure of **sorafenib**.

[a]*Faculty of Pharmacy and Medical Sciences, University of Petra, Amman, Jordan. E-mail: duaa.abuarqoub@uop.edu.jo*

[b]*Faculty of Pharmacy, Yarmouk University, Irbid, Jordan*

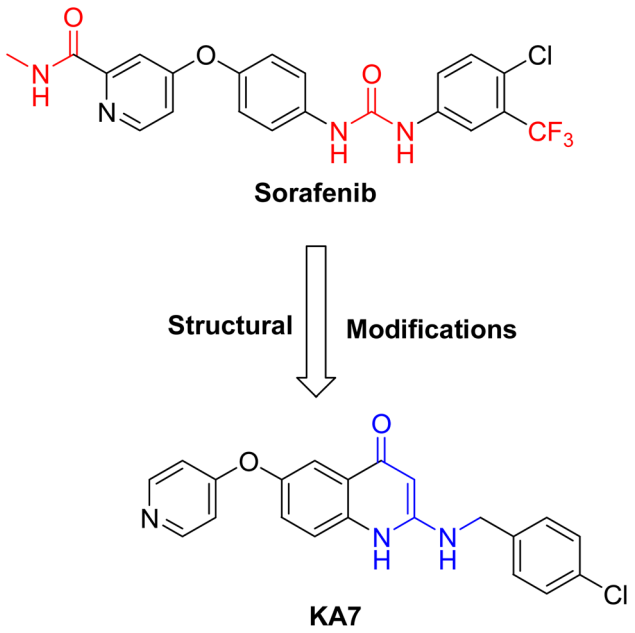


Fig. 2 **Sorafenib** and its quinolone analogue KA7.

bioavailability, reduced toxicity, and expanded activity against diverse tumor types. Therefore, considerable efforts in organic and medicinal chemistry are directed toward the development of **sorafenib**-based analogues with improved therapeutic potential against cancer progression.

Most **sorafenib** analogues retain the central urea moiety, which provides favorable hydrogen-bonding interactions with target kinases but also contributes to aggregation and plasma protein binding, causing cell toxicity and suboptimal pharmacokinetics.[13] Replacing the urea group with alternative scaffolds is a promising strategy to overcome these limitations, although challenging, as the loss of hydrogen bonding must be compensated by other structural features.

In this context, we designed a novel analogue **KA7** in which **sorafenib**'s urea moiety was replaced with a quinolone core. The new structure is a 2-amino-6-phenoxyquinoline that also carries a benzylamine group (Fig. 2).

Quinolines are privileged scaffolds in drug discovery, characterized by a fused benzene–pyridine bicyclic structure that imparts favorable electronic and steric properties. Quinoline derivatives have been widely studied for their diverse pharmacological activities, including antibacterial, antifungal, antiviral, anti-inflammatory, and anticancer effects.[14–16]

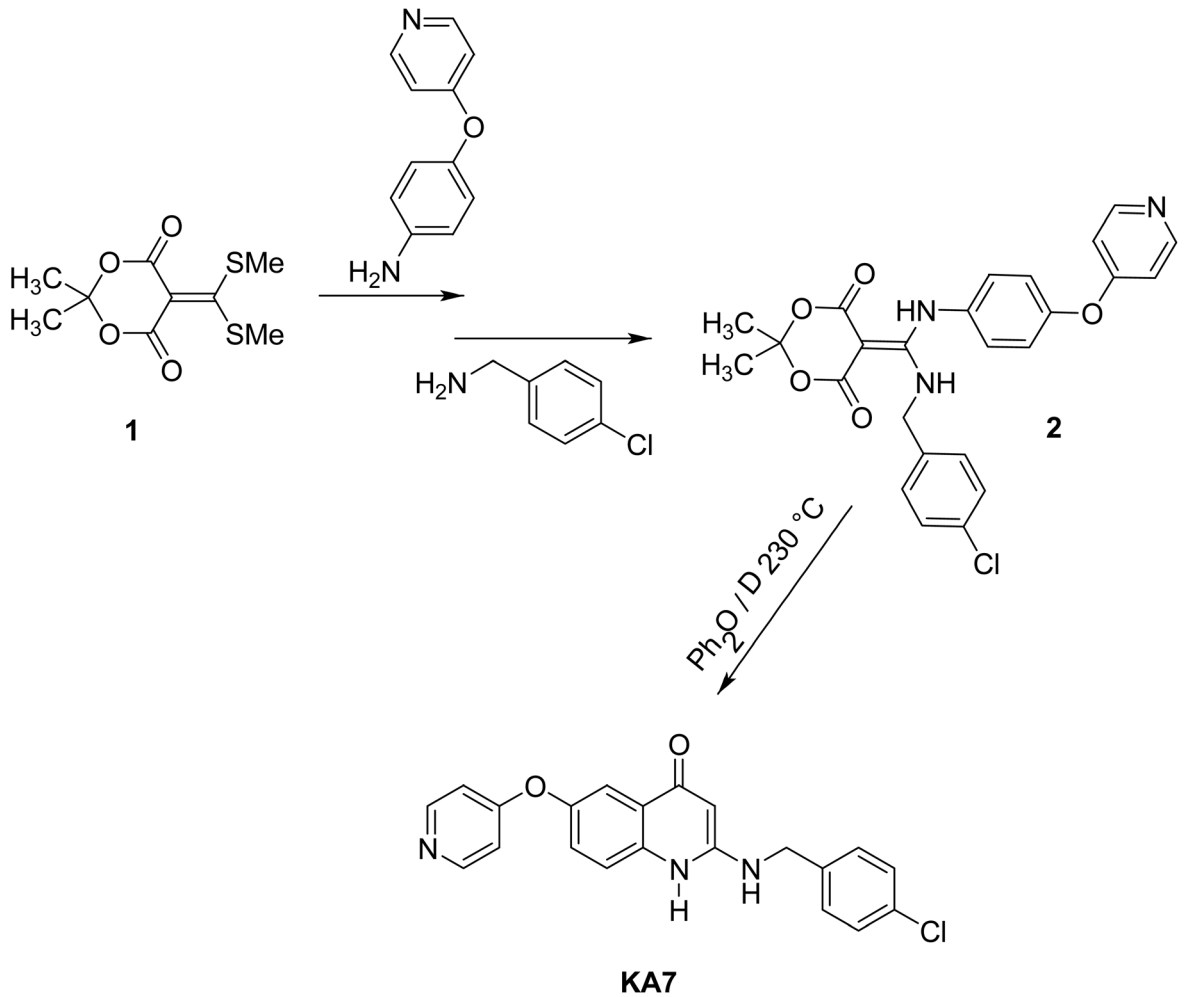


Fig. 3 General synthesis method of 2-(4-chlorobenzylamino)-6-(pyridin-4-yloxy) quinolin-4(1*H*)-one (**KA7**).

Importantly, their ability to interfere with key cellular processes relevant to tumorigenesis has made them attractive candidates for anticancer drug development.[17,18]

Herein, we report the synthesis of 2-(4-chlorobenzylamino)-6-(pyridin-4-yloxy) quinolin-4(1*H*)-one (**KA7**), a **sorafenib** analogue featuring a quinoline core. We evaluate its cytotoxic effects across a panel of human cancer cell lines, including breast (MDA-231, MCF-7), glioblastoma (U87), and lung (A549), along with normal human dermal fibroblasts (HDF) for selectivity. Furthermore, we investigate its mechanism of action through apoptosis, cell cycle and autophagy assays, as well as its immunomodulatory profile in macrophage models.

## Materials and methods

### Chemistry

In our present research 2-(4-chlorobenzylamino)-6-(pyridin-4-yloxy)quinolin-4(1*H*)-one (**KA7**) was synthesized *via* the nucleophilic displacement of SMe groups in the starting compound 5-[bis(methylsulfanyl)-methylidene]-2,2-dimethyl-1,3-dioxane-4,6-dione **1** with 4-(pyridin-4-yloxy)benzenamine and (4-chlorophenyl)methanamine, respectively to get intermediate **2**. Intermediate **2** is converted to quinoline by heating at 230 °C to give the final product **KA7** (Fig. 3).

### Experimental part

Chemicals and reagents used were purchased from Combi-Blocks, Acros Organics and Sigma-Aldrich. All reagents and chemicals used without any further purification.

All NMR spectra were acquired in deuterated DMSO using a Bruker spectrometer at 500 MHz. High-resolution mass spectra (HRMS) were obtained using an electrospray ionization technique on a Bruker Impact II mass spectrometer in positive-ion mode at 2500 V Fig. S1.

High-performance liquid chromatography (HPLC) was performed using a Thermo Fisher Scientific P1000 pump integrated into AS 3000 system, and UV 2000 detector. Separation was achieved on a C18 column (150 mm × 4.6 mm1), mobile phase 80% $CH_3OH$ and 20% Deionized water. The detection wavelength 254 nm, pump flow rate 1 mL $min^{-1}$ flow rate Fig. S2.

### Procedure

2-(4-Chlorobenzylamino)-6-(pyridin-4-yloxy) quinolin-4(1*H*)-one (**KA7**). 1 (0.40 g, 1.60 mmol) and 4-(pyridin-4-yloxy) benzenamine (0.33 g, 1.76 mmol) in 10 ml THF was heated at reflux for 1.5 h and then (4-chlorophenyl) methanamine (0.22 ml, 1.76 mmol) was added. The reaction was stirred for an additional 2 h. The THF was evaporated and the crude solid was washed with diethyl ether to yield the intermediate **2**. The intermediate **2** was heated in diphenyl ether at 230 °C for 15 minutes. The reaction mixture was cooled to room temperature then the diethyl ether was added. The resulting precipitate was filtered off to give 0.2 g (33%) of **KA7** as off-white solid.

$^1$H NMR (500 MHz, DMSO) *δ*: 10.92 (s, 1H), 8.43–6.89 (m, 11H), 5.25 (s, 1H), 4.46 (s, 2H). $^{13}$C NMR (126 MHz, DMSO) *δ*: 164.97, 151.93, 148.64, 147.92, 131.76 129.41, 128.80, 124.29, 124.21, 124.06, 123.77, 112.37, 110.64, 44.33. HRMS ESI$^+$, ([M + H]$^+$)*m/z*: calculated for $C_{21}H_{17}ClN_3O_2$ 378.1009; found, 378.0990. Fig. S3

### Cell culture

MDA-231, MCF-7, U87, A549, and THP-1 cells. All cells were donated from the cell therapy center at the University of Jordan.

MDA-231 and U87 cells were cultured in high-glucose Dulbecco's Modified Eagle Medium (DMEM) (EuroClone, Pero, Italy), while MCF-7, A549, and THP-1 cells were maintained in Roswell Park Memorial Institute (RPMI) 1640 medium (EuroClone, Italy). Both media were supplemented with 10% fetal bovine serum (FBS) (Cytiva, Marlborough, MA, USA), 1% penicillin-streptomycin, 1% l-glutamine, and 0.1% amphotericin B (EuroClone S.p.A., Pero, Italy). Cells were incubated at 37 °C in a humidified incubator with 5% $CO_2$ (Esco Lifesciences Group, Singapore) and subcultured upon reaching 70–90% confluence using trypsin-EDTA 1× in PBS (EuroClone, Pero, Italy).

### MTT assay-$IC_{50}$

5000 cells per well of the cell lines, MDA-231, MCF-7, U87, and A549, were cultured in a 96-well plate, and were treated with a serial dilution ranging from 50 to 1.5 μM to determine the $IC_{50}$. Following 72 hours of treatment, 15 μL of MTT reagent was added to each well. The plate was incubated at 37 °C for 3 hours. Later, 50 μL of the stop solution was added to each well. Absorbance was measured at 570 nm using a microplate reader (Thermo Fisher Scientific, USA).

For the calculation of $IC_{50}$ values, nonlinear regression analysis was performed using GraphPad Prism version 8.4, with logarithmic concentration plotted against viability percentage values.

### Cell death modality (apoptosis/necrosis assay)

To evaluate the impact of **KA7** on cell death, apoptosis, and necrosis were assessed in MDA-231, MCF-7, U87, and A549 cells, with **Sorafenib** used as a positive control. Initially, cells were seeded at a density of 250 000 cells per well in 6-well plates (SPL Life Sciences, Pocheon, Korea) and treated with **KA7** and **sorafenib** at the $IC_{50}$ and double the $IC_{50}$ concentrations for 72 hours. Following treatment, cells were harvested using 1× trypsin (EuroClone S.p.A., Pero, Italy), collected by centrifugation. Following, cells were stained with Annexin V and propidium iodide (Invitrogen, Carlsbad, CA, USA) according to the manufacturer's protocol and analyzed using BD Accuri™ C6 Plus flow cytometry (BD Biosciences, Franklin Lakes, NJ, USA) using FL1 filter for Annexin V signal detection and FL2 filter for PI signal detection.

### Cell cycle assay

To evaluate the impact of **KA7** on cell cycle progression, initially, MDA-231, MCF-7, U87, and A549 cells were seeded at a density of 250 000 cells per well in 6-well plates (SPL Life Sciences, Pocheon, Korea) and treated with **KA7** and **sorafenib** at the $IC_{50}$ and double the $IC_{50}$ concentrations for 72 hours. Following treatment, cells were harvested using 1× trypsin (EuroClone S.p.A., Pero, Italy), collected by centrifugation. The collected samples for the cell cycle assay were then fixed in 500

μL of cold methanol and stored at −20 °C until processing the samples. Next, samples were washed twice with PBS, resuspended in 50 μL PBS, and incubated with 150 μL of an RNase A/propidium iodide (PI) solution (NZYTech, Lisbon, Portugal; Tocris Bioscience, Bristol, UK) at final concentrations of 0.2 mg $mL^{-1}$ and 0.04 mg $mL^{-1}$, respectively. Samples were incubated in the dark for 30 min, followed by the addition of 100 μL PBS. Flow cytometry analysis was performed using BD Accuri™ C6 Plus using FL2 filter, and data were processed using FlowJo software version 10 (BD Biosciences, Franklin Lakes, NJ, USA).

### Acridine orange (AO) staining

Based on fluorescence emission, AO staining was performed to assess cellular changes following treatment MDA-231, MCF-7, U87, and A549 cells were seeded at a density of 120 000 cells per well in a 12-well plate and allowed to adhere overnight. Cells were then treated with $IC_{50}$ concentrations of **KA7** for 72 hours. After incubation, cells were washed with PBS, harvested, and collected by centrifugation, and the supernatant was discarded. The cell pellet was resuspended in 10 μM AO and incubated for 15 minutes in a dark place. Following staining, excess AO was removed by washing with PBS, and the cells were centrifuged and resuspended in 250 μL of PBS. Fluorescence analysis was performed using BD Accuri™ C6 Plus flow cytometry, with FITC and PerCP filters. Data analysis was conducted using BD Accuri™ software.

### Inflammatory response

**Differentiation and stimulation of THP-1 cells.** THP-1 cells were seeded at a density of $1 \times 10^6$ cells per well in a 6-well plate and maintained in RPMI medium (EuroClone, Italy) supplemented with 150 nM phorbol 12-myristate 13-acetate (PMA) (ChemCruz, Santa Cruz Biotechnology, Dallas, TX, USA) to promote differentiation into macrophage-like cells. Following a 24-hour incubation, the differentiated macrophages were further stimulated with 1 μg per mL lipopolysaccharide (LPS) (ChemCruz, Santa Cruz Biotechnology, Dallas, TX, USA) for an additional 24 hours to induce an inflammatory response. Cells were subsequently treated with 10 μM **KA7** and 10 μM **sorafenib**, then incubated at 37 °C in a $CO_2$ incubator for 24 hours.

**Cytokine detection using cytometric bead array (CBA).** At the end of the treatment period, culture supernatants were collected and stored at −20 °C for cytokine profiling. The levels of IL-1β, IL-6, IL-8, IL-10, IL-12p70, and TGF-β were evaluated using the cytometric bead array (CBA) kit (BD Biosciences, Franklin Lakes, NJ, USA) according to the manufacturer's protocol. Flow cytometric analysis was conducted using the BD Accuri™ C6 Plus flow cytometer (BD Biosciences, Franklin Lakes, NJ, USA) using PE filter. Cytokine concentrations were determined by interruption from a standard curve made with a freshly prepared cytokine bead mixture. The results were expressed as cytokine concentration (pg $mL^{-1}$) relative to the untreated control.

**Statistical analysis.** All statistical analyses were done using GraphPad Prism software. All experiments were done in triplicate in three independent experiments ($n = 3$). Data are presented as mean ± standard deviation (SD). Two-way ANOVA was used to evaluate apoptosis and cell cycle assays, while one-way ANOVA was used for Acridine orange and CBA assays, and the Dunnett Test for multiple comparisons between treated groups and controls for all assays.

Statistical significance was stated as $*p < 0.05$.

## Results

### Comparative cytotoxicity of KA7 and sorafenib across cancer cell lines

The MTT assay was employed to assess the inhibitory effect of the **KA7** compound on various cancer cell lines. After 72 hours of treatment, the $IC_{50}$ values for both **KA7** and **sorafenib** (SOR) were determined using the MTT assay. The results are presented in Fig. 4. As shown in Fig. 4, the $IC_{50}$ of MDA-231, U87, and A549 cells treated with **KA7** was lower compared to their treatment with **sorafenib**. The $IC_{50}$ results were (MDA-231:6.70 ± 0.78, U87:5.40 ± 0.75, and A549:4.70 ± 0.66) cells treated with **KA7** compound, while the $IC_{50}$ for cells treated with **sorafenib** were as follows: (MDA-231:9.40 ± 1.03, U87:15 ± 1.10, and A549:11 ± 1.30). Though MCF-7 treatment showed comparable $IC_{50}$ values, as $IC_{50}$ was 9.30 ± 0.97 for cells treated with **KA7** and 8.50 ± 1.30 for cells treated with **sorafenib**.

### Cell death modality (apoptosis/necrosis assay)

To investigate the impact of **KA7** on cell death modality, MDA-231, MCF-7, U87, and A549 were treated with $IC_{50}$ and double $IC_{50}$ concentrations of **KA7** or **sorafenib**, then assessed using an Annexin V/PI staining assay after 72 hours of treatment.

Our results demonstrated that, across all cell lines, there was a significant increase in the percentage of Annexin V-positive cells compared to the control untreated groups ($p < 0.05$) in all treated cell lines. The $IC_{50}$ results for the percentage of Annexin V-positive cells were as follows: for MDA-231:39.06 ± 263, MCF-7: 6.14 ± 2.14, U87:3.30 ± 0.30, and A549:16.90 ± 1.89. For the double $IC_{50}$, the results were MDA-231:36.23 ± 1.60, MCF-7: 11.98 ± 0.98, U87:7.70 ± 3.30, and A549 47.16 ± 3.80.

In the control untreated cells, the percentages of Annexin V-positive cells were as follows: MDA-231:21.11 ± 1.61, MCF-7: 3.18 ± 0.56, U87:1.06 ± 0.09, and A549:6.24 ± 0.42. For the PI-positive cells, only MDA-231 and MCF-7 cells treated with **KA7** exhibited a significant increase in the percentage of PI-positive cells compared to the control untreated cells ($p < 0.05$). Consequently, these results indicate that **KA7** induced apoptotic cell death in the treated cells.

Similarly, the **sorafenib**-treated cells showed a highly significant increase in both Annexin V-positive and PI-positive cells among all cell lines treated. The $IC_{50}$ results for Annexin V-positive cells were MDA-231:86.30 ± 0.63, MCF-7: 2.40 ± 0.40, U87:3.30 ± 0.37, and A549:77.76 ± 2.16. For the PI-positive cells, the results were MDA-231:5.80 ± 0.70, MCF-7: 12.13 ± 2.51, U87:1.96 ± 0.40, and A549:20.40 ± 2.10.

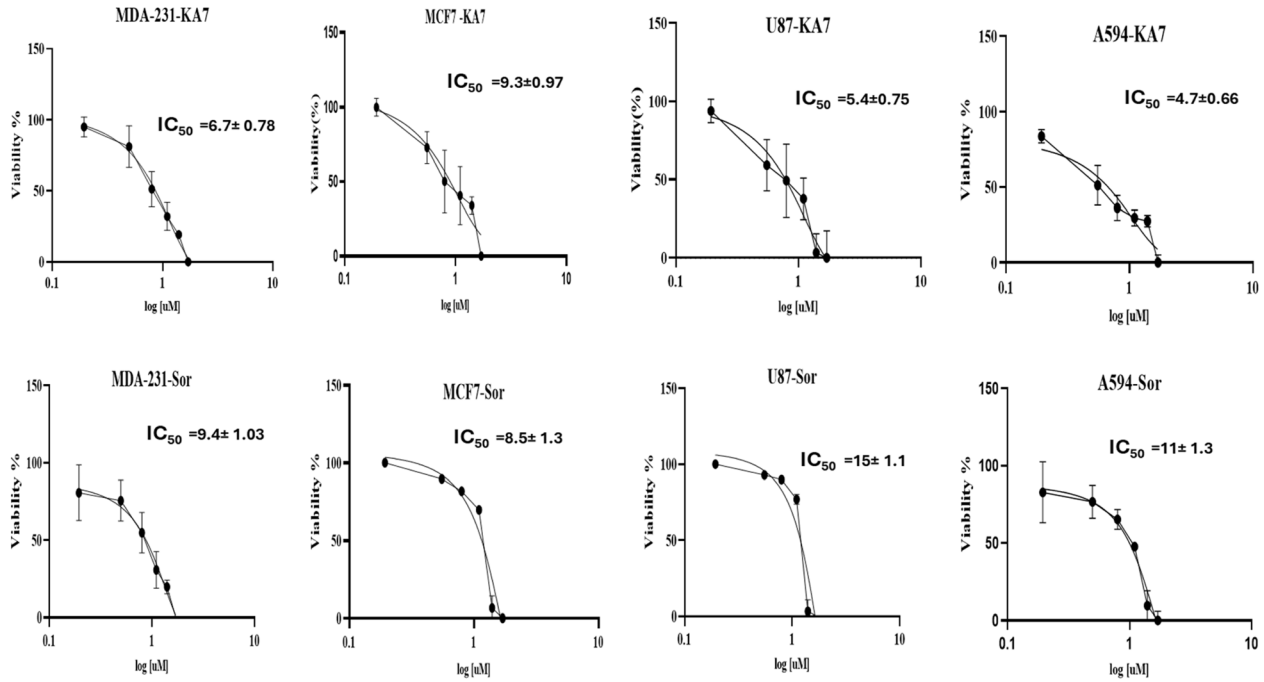


Fig. 4 $IC_{50}$ values for the cell viability after 72 hours of treatment with the KA7 compound and sorafenib (SOR). Nonlinear regression analysis was performed to calculate $IC_{50}$ values, using GraphPad Prism version 8.4, with logarithmic concentration plotted against viability percentage values.

Similar trends were observed in cells treated with double $IC_{50}$ for Annexin V-positive cells (MDA-231:80.30 ± 0.15, MCF-7: 13.00 ± 2.17, U87:7.3 ± 0.30, and A549:66.09 ± 2.06) and PI-positive cells (MDA-231:12.30 ± 0.37, MCF-7: 32.70 ± 2.52, U87:9.80 ± 1.10, and A549 29.10 ± 1.87), as shown in Fig. 5.

### Cell cycle assay

To investigate the effect of **KA7** on cell cycle progression, MDA-23, MCF-7, U87, and A549 cells were treated with $IC_{50}$ and double $IC_{50}$ concentrations of **KA7** and **sorafenib** for 72 hours.

Our results demonstrated that both **KA7** and **sorafenib** caused an arrest in the G1 phase of treated cells, resulting in a significant reduction in the percentage of cells progressing to the G2 phase across all cell lines.

The results for **KA7** at $IC_{50}$ were as follows: for MDA-231 cells, the percentage was 76.29 ± 1.33; for MCF-7 cells, it was 79.50 ± 0.93; for U87 cells, it was 85.5 ± 0.50; and for A549, it was 58.70 ± 1.93. For cells treated with double **KA7** $IC_{50}$, the percentages were: MDA-231:83.30 ± 3.0, MCF-7: 87.58 ± 0.58, U87:85.50 ± 0.58, and A549:90.40 ± 0.40. In contrast, the control group of untreated cells showed the following percentages: MDA-231 at 36.51 ± 3.30, MCF-7 at 41.12 ± 1.49, U87 at 46.30 ± 3.50, and A549 at 67.70 ± 2.29.

Similarly, G1 arrest was observed in cells treated with **sorafenib** at $IC_{50}$, with results as follows: MDA-231 at 89.20 ± 7.87, MCF-7 at 87.90 ± 1.53, and U87 at 66.17 ± 1.10. For double $IC_{50}$ doses of **sorafenib**, the results were: MDA-231 at 92.30 ± 1.36, MCF-7 at 85.40 ± 4.14, and U87 at 69.02 ± 1.02. However, in the case of A549 cells treated with $IC_{50}$ and double $IC_{50}$ of **sorafenib**, the cells were arrested in the G2 phase, and the percentages of cells in the G1 and S phases decreased significantly, as illustrated in Fig. 6.

### Acridine orange (AO) staining

To assess autophagic activity, cells were treated with $IC_{50}$ values of the **KA7** compound for 72 hours. Following the treatment, the cells were stained with acridine orange to evaluate autophagic activity.

The results indicated a significant increase in the percentage of acridine orange-positive cells across all cell lines. Specifically, the percentages were: MDA-231:25.70% ± 4.04, MCF-7: 23.03% ± 3.60, U87:13.40% ± 2.20, and A549:33.32% ± 1.15. These values were notably higher when compared to the control untreated groups, which showed the following percentages: MDA-231:3.30% ± 0.40, MCF-7: 1.963% ± 0.55, U87:1.90% ± 0.43, and A549:4.96% ± 1.41. The findings are illustrated in Fig. 7.

### Inflammatory response

To evaluate the inflammatory responses of the **KA7** compound, THP-1 cells were infected with lipopolysaccharide (LPS) and treated with 10 μM of **KA7** or **sorafenib**. The secretion levels of cytokines were measured using multiplex flow cytometry.

The results indicated a decrease in the levels of pro-inflammatory cytokines, including IL-1β, TNF-α, and IL-6, in cells treated with **KA7** and **sorafenib** (SOR). The results were as follows: IL-1β: Control: 235.99 ± 36.50 **KA7**: 14.77 ± 1.04, SOR: 2.76 ± 2.77 pg $ml^{-1}$. IL-6: Control: 936.35 ± 117, **KA7**: 176.32 ± 12.80, SOR: 28.4 ± 4.16 pg $ml^{-1}$. TNF-α: Control: 268.05 ± 38.04 pg $ml^{-1}$, **KA7**: 4.06 ± 0.05 pg $ml^{-1}$, SOR: 4.70 ± 0.46 pg $ml^{-1}$.

Additionally, the secretion levels of anti-inflammatory cytokines IL-10 and IL-8 showed a significant increase ($p < 0.05$). The levels were as follows: IL-10:Control: 0.70 ± 0.11, **KA7**: 4.26 ± 0.12, SOR: 5.39 ± 0.14 pg $ml^{-1}$. IL-8:Control: 680.14 ± 121.40,

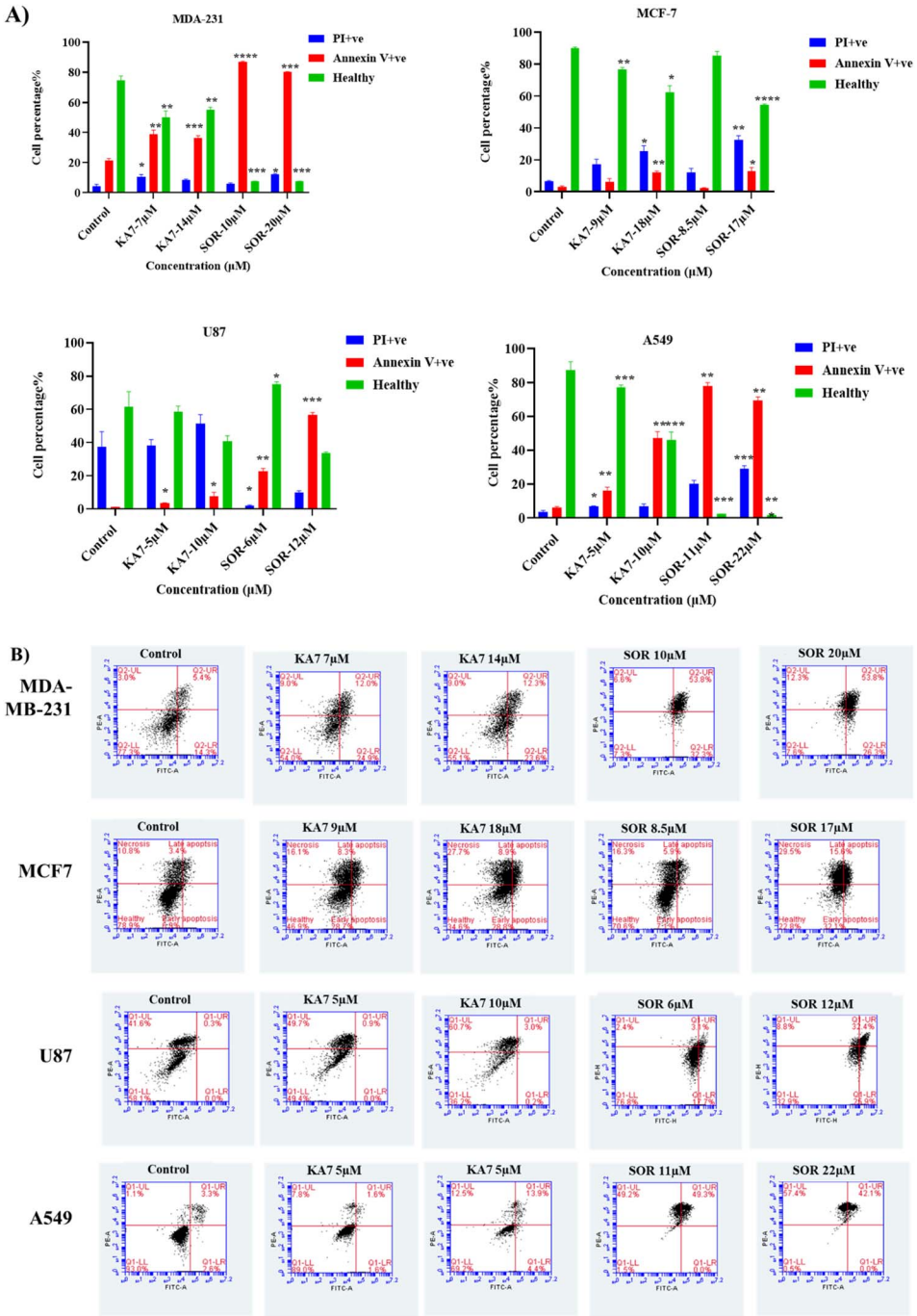


Fig. 5 (A) Flow cytometric analysis and (B) Flow cytometric dot plots of the percentages of healthy and dead cells (apoptotic/necrotic cells) of MDA-231, MCF-7, U87, and A549 cells following 72 hours of treatment with **KA7** and **sorafenib** (SOR) at $IC_{50}$ and double the $IC_{50}$ concentrations (μM) compared to untreated controls. Data are presented as mean ± SD. Statistical significance was determined using two-way ANOVA (*$p$ < 0.05).

**KA7:** 755.48 ± 25.40 pg ml$^{-1}$, SOR: 1363.03 ± 62.60 pg ml$^{-1}$. Whereas for IL-12p70 no statistical difference was observed among all treatment groups: IL-12p70: Control: 7.42 ± 1.94, **KA7:** 7.69 ± 0.06 pg ml$^{-1}$, SOR: 7.84 ± 0.064 pg ml$^{-1}$.

Consequently, these results indicate the anti-inflammatory potential of the **KA7** compound, which is comparable to the effects of **sorafenib**, as illustrated in Fig. 8.

## Discussion

In this study, a novel **sorafenib** analogue **KA7** was synthesized and characterized, in which the urea moiety was replaced with a quinolone scaffold. **KA7** demonstrated potent cytotoxic effects across multiple cancer cell lines, including breast (MDA-231, MCF-7), glioblastoma (U87), and lung (A549). Notably, **KA7** was approximately twice as potent as **sorafenib** against U87 cells

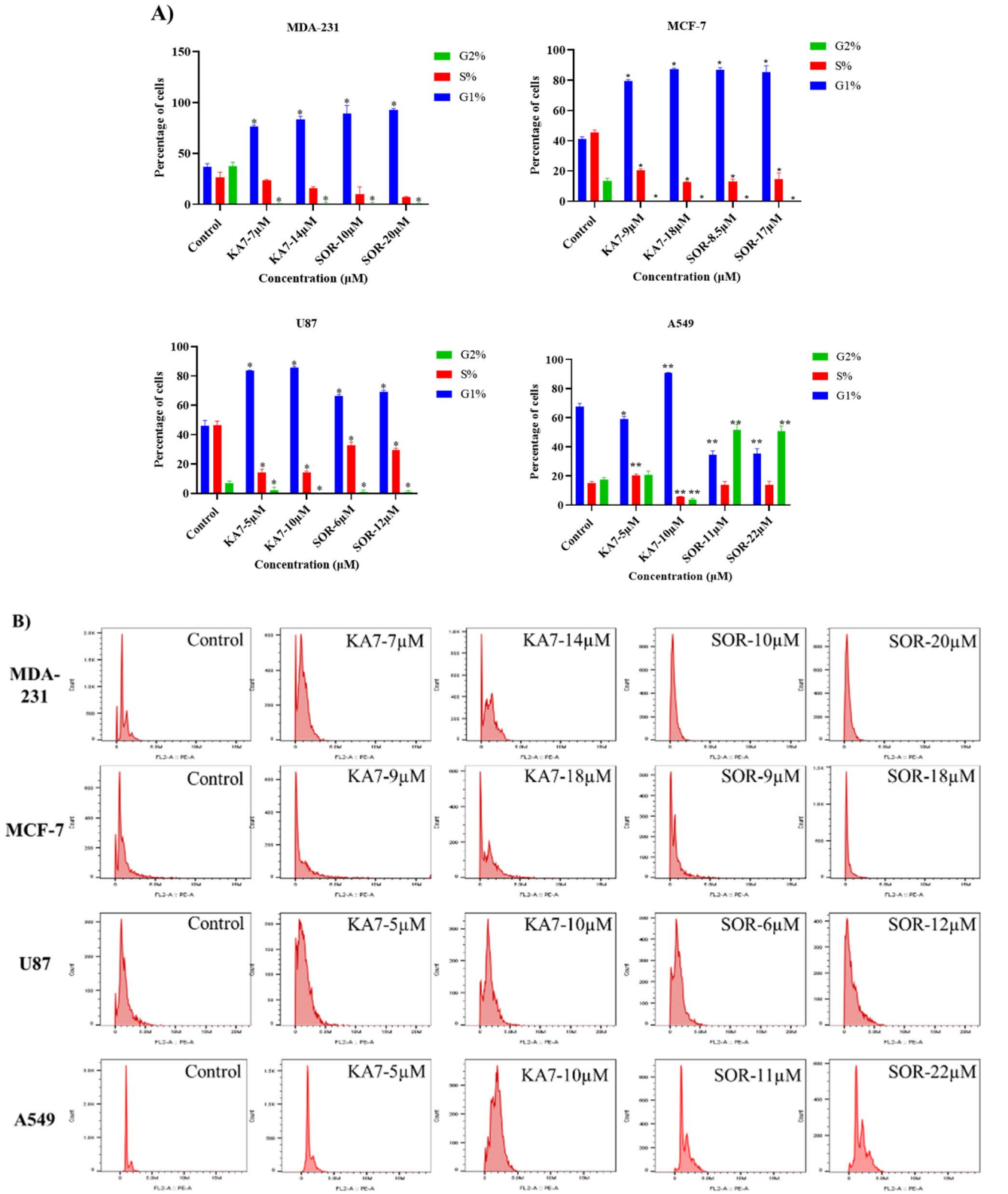


Fig. 6 (A) Cell cycle analysis and (B) cell cycle flow cytometric histograms of MDA-231, MCF-7, U87, and A549 cells following 72 hours of treatment with **KA7** and **sorafenib** (SOR) at $IC_{50}$ and double the $IC_{50}$ concentrations (μM) compared to untreated controls. Data are presented as mean ± SD. Statistical significance was determined using two-way ANOVA (*$p < 0.05$).

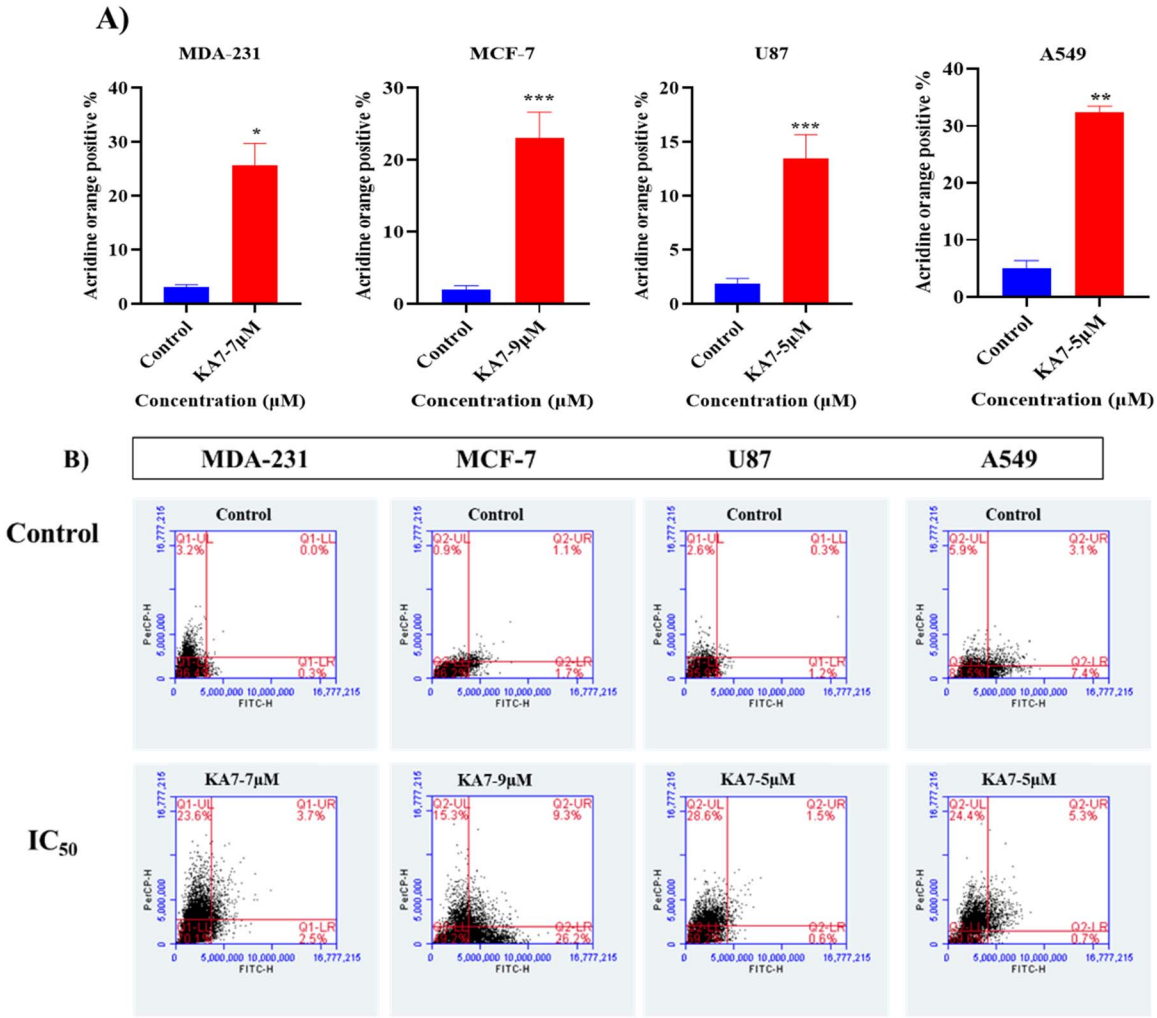


Fig. 7 (A) Acridine orange analysis and (B) acridine orange flow cytometric results of treated MDA-231, MCF-7, U87, and A549 cells for 72 hours with **KA7** and **sorafenib** (SOR) at $IC_{50}$ concentrations (μM) compared to untreated controls. Data are presented as mean ± SD. Statistical significance was determined using one-way ANOVA (*$p < 0.05$).

and three times more potent against A549 cells. These findings suggest that **KA7** retains broad anticancer activity similar to **sorafenib**, while showing enhanced potency in selected cancer models.

In line with our strategy of replacing **sorafenib**'s aryl urea moiety, other studies have explored alternative scaffolds such as 1,2,3-triazoles. For example, a series of triazole-containing **sorafenib** analogues, in which the urea group was substituted by a 1,2,3-triazole ring linking a phenoxy fragment, was synthesized *via* Huisgen 1,3-dipolar cycloaddition and nucleophilic aromatic substitution.[19] Cytotoxicity studies against hepatocellular carcinoma cell lines revealed that most analogues showed only moderate to weak activity against HepG2 cells (best $IC_{50} = 61.6 \pm 5.2$ μM). However, several compounds displayed notable inhibitory activity against Huh7 cells, with the *p-tert*-butylphenoxy analogue achieving significant potency ($IC_{50} = 5.67 \pm 0.57$ μM). Importantly, this compound demonstrated a high selectivity index (SI > 17.6), which was markedly superior to that of **sorafenib** (SI = 6.73), underscoring the value of aryl urea replacement strategies in generating analogues with improved potency and safety profiles.

Similar efforts have also focused on replacing **sorafenib**'s aryl urea moiety with pyrazole scaffolds. In one study, four series of pyrazole-containing **sorafenib** derivatives were synthesized and tested for cytotoxicity against A549, HepG2, MCF-7, and PC-3 cancer cell lines. Among them, one compound, bearing a 3-bromo substitution at the C-3 position of the pyrazole ring, emerged as the most potent. It exhibited $IC_{50}$ values of 2.84 ± 0.78 μM (A549), 1.85 ± 0.03 μM (HepG2), and 1.96 ± 0.28 μM (MCF-7), which were comparable to or better than **sorafenib**.[20] The superior cytotoxicity of this compound compared to unsubstituted derivatives suggests that C-3 substitutions play a critical role in the structural optimization of **sorafenib** analogues. In addition to triazole- and pyrazole-based analogues, chalcone derivatives of **sorafenib** have also attracted significant attention due to their broad biological activities.[21–23] Wang *et al.* reported that replacing the aryl urea group with a chalcone moiety produced derivatives with equal or superior potency to **sorafenib** against A549,

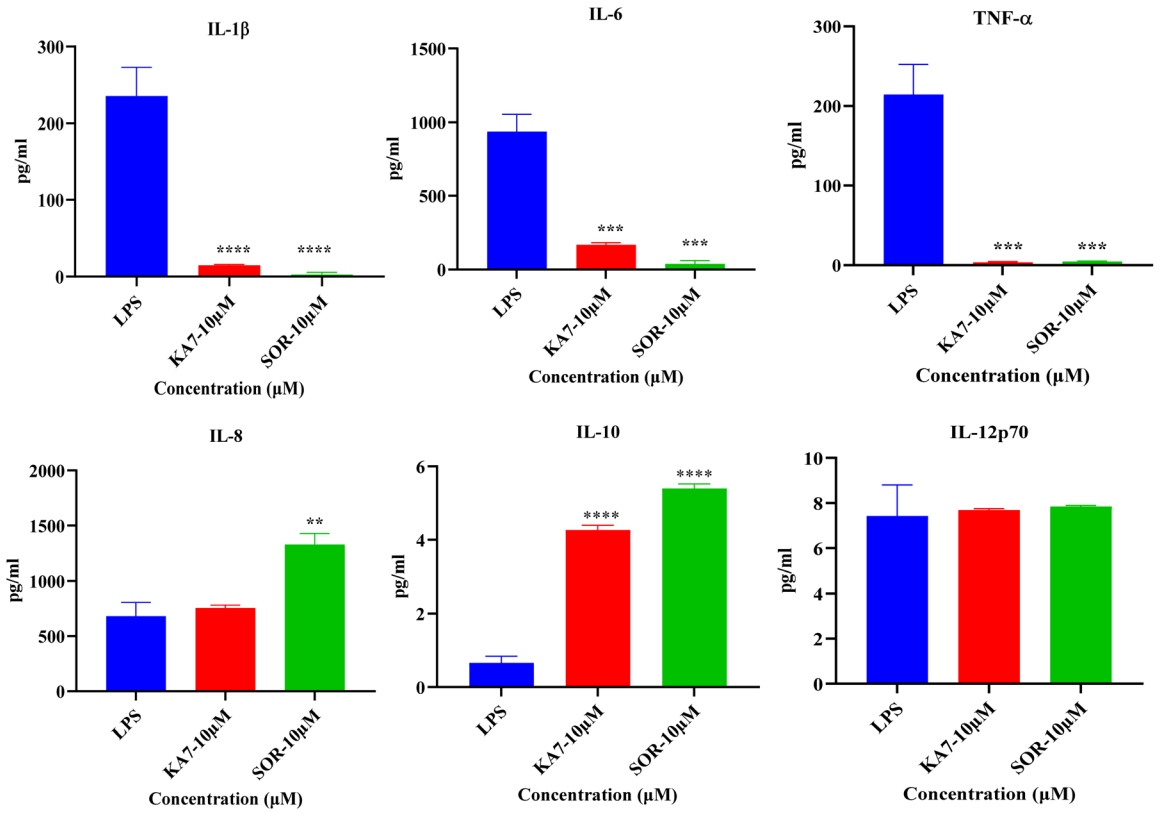


Fig. 8 Inflammatory response of macrophage cells, activated with LPS and treated with 10 μM **KA7** and 10 μM **sorafenib** (SOR) for 72 hours, and compared to the control untreated. Measurement of the secretion level of cytokines at the protein level, measured by cytometric bead array (CBA)-flow cytometry. A One-way ANOVA test was used for statistical analysis. Bars represent means ± SD (*$p$ < 0.05).

HepG2, MCF-7, and PC-3 cell lines, including one compound with sub-micromolar activity against HepG2 ($IC_{50} = 0.56 \pm 0.83$ μM).[24] Collectively, these findings highlight that replacing the aryl urea moiety with alternative scaffolds, such as pyrazole, triazole, or chalcone rings, can enhance antitumor potency. Our quinolone-based analogue **KA7** follows this rationale, demonstrating improved activity against selected cancer cell lines and reinforcing scaffold engineering as a promising strategy for optimizing **sorafenib** analogues. Substituting **sorafenib**'s urea moiety with a quinolone framework represents a rational approach to address the pharmacokinetic and toxicity limitations of urea-containing kinase inhibitors, while preserving potency and, in some cases, enhancing activity against specific cancer types.

Flow cytometry analysis demonstrated that **KA7** induced significant apoptosis across all tested cancer cell lines, as evidenced by increased Annexin V-positive populations. This aligns with **sorafenib**'s established mechanism as a multikinase inhibitor, which promotes apoptosis through inhibition of the Raf–MEK–ERK and mTOR pathways, downregulation of anti-apoptotic proteins such as Mcl-1 and survivin, and upregulation of pro-apoptotic mediators like Redd1.[25–27] **Sorafenib** has also been reported to trigger mitochondrial fragmentation, which facilitates cytochrome c release and activates caspase-dependent apoptosis.[28,29] Several **sorafenib** analogues similarly promote apoptotic cell death through related mechanisms.[30–33] In addition, **KA7** induced a marked arrest in the G1 phase of the cell cycle, thereby limiting progression to the G2/M phase. Notably, **sorafenib** has been shown to cause G2 arrest in A549 cells, whereas **KA7** predominantly induced G1 arrest, suggesting subtle mechanistic distinctions between the two compounds. Future studies should investigate the involvement of key cell cycle regulatory proteins such as cyclin D1, CDK4/6, p21, and p27, which could help clarify the molecular basis of **KA7**-induced G1 arrest.

In addition to apoptosis and cell cycle arrest, our findings revealed that **KA7** also triggered autophagy, as demonstrated by acridine orange staining. Autophagy is a double-edged process in cancer: while it can function as a pro-survival mechanism under stress, excessive activation may lead to autophagic cell death.[34] Consistent with our observations, **sorafenib** has been widely reported to induce autophagy in cancer cells.[35–38] For example, in prostate cancer, **sorafenib**-induced formation of Atg5-deficient autophagosomes promoted the interaction of p62 with RIPK, leading to necroptotic cell death,[36] whereas in renal cancer cells, **sorafenib** activated a cytoprotective form of autophagy that interfered with the effectiveness of **sorafenib**-mediated apoptosis.[35] These contrasting reports underscore the context-dependent role of autophagy in cancer therapy. Our data suggest that **KA7** shares this autophagy-inducing property, but further studies are needed to determine whether **KA7**-mediated autophagy enhances cell death or contributes to adaptive resistance. Future investigations should examine the expression of key autophagy regulators such as LC3-II, Beclin-1,

and p62/SQSTM1 to elucidate the molecular mechanisms underlying **KA7**-induced autophagy.

An important observation of this study was the immunomodulatory activity of **KA7**. In LPS-stimulated THP-1 macrophages, both **KA7** and **sorafenib** significantly reduced the secretion of pro-inflammatory cytokines (IL-1β, TNF-α, IL-6) while enhancing anti-inflammatory mediators (IL-8 and IL-10). These effects are consistent with previous reports describing **sorafenib**'s ability to modulate the tumor microenvironment and immune signaling.[39–41] Elevated TNF-α levels have been implicated in driving epithelial–mesenchymal transition and promoting **sorafenib** resistance in hepatocellular carcinoma cells.[42] The ability of **KA7** to downregulate TNF-α may therefore represent an important mechanism for overcoming resistance and improving therapeutic outcome. By combining this anti-inflammatory activity with direct cytotoxic effects, **KA7** could reduce tumor-promoting inflammation while reinforcing antitumor immunity. This dual mechanism underscores **KA7** as a promising candidate for incorporation into combination strategies with immunotherapeutic agents.

All of these findings point to **KA7** as a viable structural scaffold inspired by **sorafenib** that needs more refinement. Although **KA7** showed increased potency in some cell lines, these findings should be considered model-dependent and preliminary rather than a sign of widespread therapeutic superiority. As a result, **KA7** represents a lead molecule for further mechanistic characterization, *in vivo* validation, and structure–activity refinement.

Furthermore, given its immunomodulatory profile, **KA7** should be investigated in tumor-immune co-culture systems and *in vivo* models that better reflect the complexity of the tumor microenvironment.

## In conclusion

The effective synthesis of **KA7**, a quinolone-based analogue of **sorafenib**, is highlighted in this paper. It showed improved cytotoxicity against a number of cancer cell lines, including breast cancer, lung cancer, and glioblastoma cell models. Its capacity to trigger autophagy, induce apoptosis, and cause G1 phase cell cycle arrest was validated by mechanistic investigations. Crucially, **KA7** had an immunomodulatory profile, lowering pro-inflammatory cytokines and increasing anti-inflammatory mediators, which may have both immunoregulatory and anticancer effects. All things considered, these results indicate that replacing the urea moiety with a quinolone scaffold yields **KA7** as a promising structural analogue rather than a confirmed superior therapeutic alternative to **sorafenib**. **KA7** should therefore be viewed as a lead candidate for further optimization and preclinical evaluation, with particular focus on improving selectivity, clarifying target engagement, and determining its translational potential.

## Author contributions

D. A. designed and planned the experiments. A. A. worked out the chemistry part. M. M., H. K., and N. A. worked out the biological part. A. H. took the lead in writing the manuscript. All authors provided critical feedback and helped shape the research, analysis, and manuscript.

## Conflicts of interest

The authors declare no conflict of interest.

## Data availability

The data supporting this article have been included as part of the supplementary information (SI). Supplementary information is available. See DOI: https://doi.org/10.1039/d5ra07478a.

## Acknowledgements

The authors would like to express their gratitude to the University of Petra for support and funding (research no. 20/4/2024).

## References

1 B. Escudier, M. D. Michaelson, R. J. Motzer, T. E. Hutson, J. I. Clark, H. Y. Lim, E. Porfiri, P. Zalewski, G. Kannourakis, M. Staehler, J. Tarazi, B. Rosbrook, L. Cisar, S. Hariharan, S. Kim and B. I. Rini, *Br. J. Cancer*, 2014, **110**, 2821–2828.
2 W. Jeong, J. H. Doroshow and S. Kummar, *Curr. Probl. Cancer*, 2013, **37**, 110–144.
3 J. M. Llovet, S. Ricci, V. Mazzaferro, P. Hilgard, E. Gane, J. F. Blanc, A. C. de Oliveira, A. Santoro, J. L. Raoul, A. Forner, M. Schwartz, C. Porta, S. Zeuzem, L. Bolondi, T. F. Greten, P. R. Galle, J. F. Seitz, I. Borbath, D. Häussinger, T. Giannaris, M. Shan, M. Moscovici, D. Voliotis and J. Bruix, *N. Engl. J. Med.*, 2008, **359**, 378–390.
4 L. Rimassa and A. Santoro, *Expert Rev. Anticancer Ther.*, 2009, **9**, 739–745.
5 P. T. White and M. S. Cohen, *Expert. Opin. Drug. Discov.*, 2015, **10**, 427–439.
6 S. M. Wilhelm, L. Adnane, P. Newell, A. Villanueva, J. M. Llovet and M. Lynch, *Mol. Cancer Ther.*, 2008, **7**, 3129–3140.
7 D. Strumberg, *Drugs Today (Barc)*, 2005, **41**, 773–784.
8 S. Wilhelm, C. Carter, M. Lynch, T. Lowinger, J. Dumas, R. A. Smith, B. Schwartz, R. Simantov and S. Kelley, *Nat. Rev. Drug. Discov.*, 2006, **5**, 835–844.
9 T. B. Lowinger, B. Riedl, J. Dumas and R. A. Smith, *Curr. Pharm. Des.*, 2002, **8**, 2269–2278.
10 Z. Zhang, B. Niu, J. Chen, X. He, X. Bao, J. Zhu, H. Yu and Y. Li, *Biomaterials*, 2014, **35**, 4565–4572.
11 M. Baron Toaldo, V. Salvatore, S. Marinelli, C. Palamà, M. Milazzo, L. Croci, L. Venerandi, M. Cipone, L. Bolondi and F. Piscaglia, *Mol Imaging Biol*, 2015, **17**, 29–37.
12 L. S. Wood, *Clin. J. Oncol. Nurs.*, 2009, **13**, 13–18.
13 M. Ilakiyalakshmi and A. A. Napoleon, *Arabian J. Chem.*, 2022, **15**, 104168.
14 I. Dine, E. Mulugeta, Y. Melaku and M. Belete, *RSC Adv.*, 2023, **13**, 8657–8682.

15 P. S. Dube, L. J. Legoabe and R. M. Beteck, *Mol. Diversity*, 2023, **27**, 1501–1526.
16 T. D. M. Pham, Z. M. Ziora and M. A. T. Blaskovich, *Medchemcomm*, 2019, **10**, 1719–1739.
17 M. Ilakiyalakshmi and A. Napoleon, *Arabian J. Chem.*, 2022, **15**, 104168.
18 S. Jain, V. Chandra, P. Kumar Jain, K. Pathak, D. Pathak and A. Vaidya, *Arabian J. Chem.*, 2019, **12**, 4920–4946.
19 S. Palakhachane, Y. Ketkaew, N. Chuaypen, J. Sirirak, J. Boonsombat, S. Ruchirawat, P. Tangkijvanich, A. Suksamrarn and P. Limpachayaporn, *Bioorg. Chem.*, 2021, **112**, 104831.
20 M. Wang, S. Xu, H. Lei, C. Wang, Z. Xiao, S. Jia, J. Zhi, P. Zheng and W. Zhu, *Bioorg. Med. Chem.*, 2017, **25**, 5754–5763.
21 Y. Ouyang, J. Li, X. Chen, X. Fu, S. Sun and Q. Wu, *Biomolecules*, 2021, **11**, 894.
22 J. S. Dhaliwal, S. Moshawih, K. W. Goh, M. J. Loy, M. S. Hossain, A. Hermansyah, V. Kotra, N. Kifli, H. P. Goh, S. K. S. Dhaliwal, H. Yassin and L. C. Ming, *Molecules*, 2022, **27**, 7062.
23 M. Naveed, A. Abid, T. Aziz, A. Saleem, A. Arshad, K. Javed, H. M. Rehman, G. Nabi, M. Al-Harbi and A. F. Alasmari, *Sci. Rep.*, 2025, **15**, 3917.
24 M. Wang, S. Xu, C. Wu, X. Liu, H. Tao, Y. Huang, Y. Liu, P. Zheng and W. Zhu, *Bioorg. Med. Chem. Lett.*, 2016, **26**, 5450–5454.
25 Y. S. Kim, H. O. Jin, S. K. Seo, S. H. Woo, T. B. Choe, S. An, S. I. Hong, S. J. Lee, K. H. Lee and I. C. Park, *Biochem. Pharmacol.*, 2011, **82**, 216–226.
26 L. Liu, Y. Cao, C. Chen, X. Zhang, A. McNabola, D. Wilkie, S. Wilhelm, M. Lynch and C. Carter, *Cancer Res.*, 2006, **66**, 11851–11858.
27 X. Wang, R. Hu, Z. Song, H. Zhao, Z. Pan, Y. Feng, Y. Yu, Q. Han and J. Zhang, *Cancer Lett.*, 2022, **547**, 215880.
28 X. Zhao, C. Tian, W. M. Puszyk, O. O. Ogunwobi, M. Cao, T. Wang, R. Cabrera, D. R. Nelson and C. Liu, *Lab. Invest.*, 2013, **93**, 8–19.
29 J. Fernando, P. Sancho, C. M. Fernández-Rodriguez, J. L. Lledó, L. Caja, J. S. Campbell, N. Fausto and I. Fabregat, *J. Cell. Physiol.*, 2012, **227**, 1319–1325.
30 K. F. Chen, W. T. Tai, J. W. Huang, C. Y. Hsu, W. L. Chen, A. L. Cheng, P. J. Chen and C. W. Shiau, *Eur. J. Med. Chem.*, 2011, **46**, 2845–2851.
31 J. H. Chu, C. R. Zhao, Z. Y. Song, R. Q. Wang, Y. Z. Qin, W. B. Li and X. J. Qu, *Biomed. Pharmacother.*, 2014, **68**, 335–341.
32 P. Yu, L. Ye, H. Wang, G. Du, J. Zhang, J. Zhang and J. Tian, *Tumour. Biol.*, 2015, **36**, 2143–2153.
33 A. T. Wecksler, S. H. Hwang, H. I. Wettersten, J. E. Gilda, A. Patton, L. J. Leon, K. L. Carraway 3rd, A. V. Gomes, K. Baar, R. H. Weiss and B. D. Hammock, *Anticancer Drugs*, 2014, **25**, 433–446.
34 J. M. Mulcahy Levy and A. Thorburn, *Cell. Death. Differ.*, 2020, **27**, 843–857.
35 B. Zheng, H. Zhu, D. Gu, X. Pan, L. Qian, B. Xue, D. Yang, J. Zhou and Y. Shan, *Biochem. Biophys. Res. Commun.*, 2015, **459**, 234–239.
36 P. Kharaziha, D. Chioureas, G. Baltatzis, P. Fonseca, P. Rodriguez, V. Gogvadze, L. Lennartsson, A. C. Björklund, B. Zhivotovsky, D. Grandér, L. Egevad, S. Nilsson and T. Panaretakis, *Oncotarget*, 2015, **6**, 37066–37082.
37 W. T. Tai, C. W. Shiau, H. L. Chen, C. Y. Liu, C. S. Lin, A. L. Cheng, P. J. Chen and K. F. Chen, *Cell. Death. Dis.*, 2013, **4**, e485.
38 Q. Yang, L. Gao, X. Huang, J. Weng, Y. Chen, S. Lin and Q. Yin, *Exp. Ther. Med.*, 2021, **22**, 980.
39 J. C. Lin, C. L. Liu, J. J. Lee, T. P. Liu, W. C. Ko, Y. C. Huang, C. H. Wu and Y. J. Chen, *Int. Immunopharmacol.*, 2013, **15**, 333–339.
40 X. Li, M. Xu, J. Shen, Y. Li, S. Lin, M. Zhu, Q. Pang, X. Tan and J. Tang, *Cell. Death. Discov.*, 2022, **8**, 281.
41 S. Martens, M. Jeong, W. Tonnus, F. Feldmann, S. Hofmans, V. Goossens, N. Takahashi, J. H. Bräsen, E. W. Lee, P. Van der Veken, J. Joossens, K. Augustyns, S. Fulda, A. Linkermann, J. Song and P. Vandenabeele, *Cell. Death. Dis.*, 2017, **8**, e2904.
42 W. Tan, X. Luo, W. Li, J. Zhong, J. Cao, S. Zhu, X. Chen, R. Zhou, C. Shang and Y. Chen, *EBioMedicine*, 2019, **40**, 446–456.